scientific reports

Check for updates

OPEN

Defluorination and adsorption of tetrafluoroethylene (TFE) on TiO_2(110) and Cr_2O_3(0001)

Jessiel Siaron Gueriba[1,2,3]✉, Nur Ellina Annisa Salehuddin[1,4], Wilson Agerico Diño[1,5]✉, Kiminori Washika[6]✉, Hiroshi Nakamura[7] & Tatsumi Kawafuchi[6]

Here, we show that metal oxide surfaces catalyze the formation of intermediate defluorinated tetrafluoroethylene (TFE) radicals, resulting in enhanced binding on the corresponding metal oxide surfaces. We attribute the preferential adsorption and radical formation of TFE on Cr_2O_3(0001) relative to TiO_2(110) to the low oxygen coordination of Cr surface atoms. This hints at a possible dependence of the TFE binding strength to the surface stoichiometry of metal-oxide surfaces.

Being able to join dissimilar materials (cf., e.g., Refs.[1–4] and references therein) is a key enabling technology to innovative and sustainable materials design for industrial applications. Some notable examples include: polymer-metal composites for bio-prosthetics and medical tools[1,2]; polymer-functionalized metal oxide surfaces for specialized applications[3–7]; polymers passivating metal oxide defects to increase carrier efficiency for better optoelectronic materials[8,9]; and polytetrafluoroethylene (PTFE) used as fluorine sources to form oxyfluoride surfaces and functionalize metal-oxides towards the realization of superconductors[10]. All of these applications fundamentally start with polymer adhesion on metal surfaces.

Two of the most commonly used metals for industrial applications are titanium and stainless steel, due to their notable physical properties, e.g., being lightweight and less susceptible to corrosion. In actual applications, these metals are exposed to oxidizing agents in the environment such as O_2 or water vapor, hence, they still manifest a thin layer of metal oxide surface. For example, on stainless steel surfaces, a layer of Cr_2O_3 forms as a protective coating against further oxidation[11]. Similarly, TiO_2 thin layers form on the surface of titanium, enhancing its biocompatibility for medical purposes[12]. Studies also show that the formation of thin metal oxide surfaces enhances binding to other metals and insulating polymers through welding or irradiation of the surface[11–15]. Here, we show the role of the reactivity of these thin metal oxide films to chemically bind with TFE.

In the following, we present results of our study on the adsorption of tetrafluoroethylene (TFE) on TiO_2(110) and Cr_2O_3(0001). We found TiO_2(110) inert and Cr_2O_3(0001) active to TFE (molecular) adsorption. This can be attributed to the nature of the surface metal atoms and the corresponding oxygen coordination. Furthermore, we found that defluorination of TFE promotes adsorption on both TiO_2(110) and Cr_2O_3(0001). These results indicate the role of the surface as a catalyst to form intermediate TFE radicals and promote adsorption on metal-oxide surfaces. Thus, the possibility of joining dissimilar materials (in this case polymer and metal-oxide surface).

Results and discussions

Molecular Adsorption of TFE on TiO_2(110) and Cr_2O_3(0001). In Fig. 1, we see weak (ca. – 0.07 eV, Configuration 1) molecular adsorption of TFE monomer on TiO_2(110) and strong (ca. – 1.38 eV, Configuration 1) adsorption on Cr_2O_3(0001). We find the adsorbed TFE retaining its planar structure, negligibly modified by TiO_2(110). These results and observations could be compared with previous studies showing an inert TiO_2 towards fluorination from PTFE forming surface oxyfluorides[10]. On the other hand, we find a relatively stronger binding for TFE adsorbed on Cr-terminated Cr_2O_3(0001), with the molecular plane tilted relative to the surface axis. We found that molecular adsorption of TFE on both metal oxide surfaces does not result in any significant

[1]Department of Applied Physics, Osaka University, Suita, Osaka 565-0871, Japan. [2]Department of Physics, De La Salle University, 2401 Taft Avenue, 0922 Manila, Philippines. [3]Institute of Laser Engineering, Osaka University, Suita, Osaka 565-0871, Japan. [4]Department of Chemical Sciences, Faculty of Science and Technology, Universiti Kebangsaan Malaysia, 43600 Bangi, Selangor, Malaysia. [5]Center for Atomic and Molecular Technologies, Osaka University, Suita, Osaka 565-0871, Japan. [6]Laser Technology Laboratory, Hirotec Co., Ltd, 5-2-1 Ishiuchiminami, Saeki-ku, Hiroshima 731-5197, Japan. [7]Research and Development Division, Technology Development Department, Charmant Inc., 6-8 Kawasari, Sabae, Fukui 916-0088, Japan. ✉email: jessiel@ile.osaka-u.ac.jp; wilson@dyn.ap.eng.osaka-u.ac.jp; washika@hirotec.co.jp

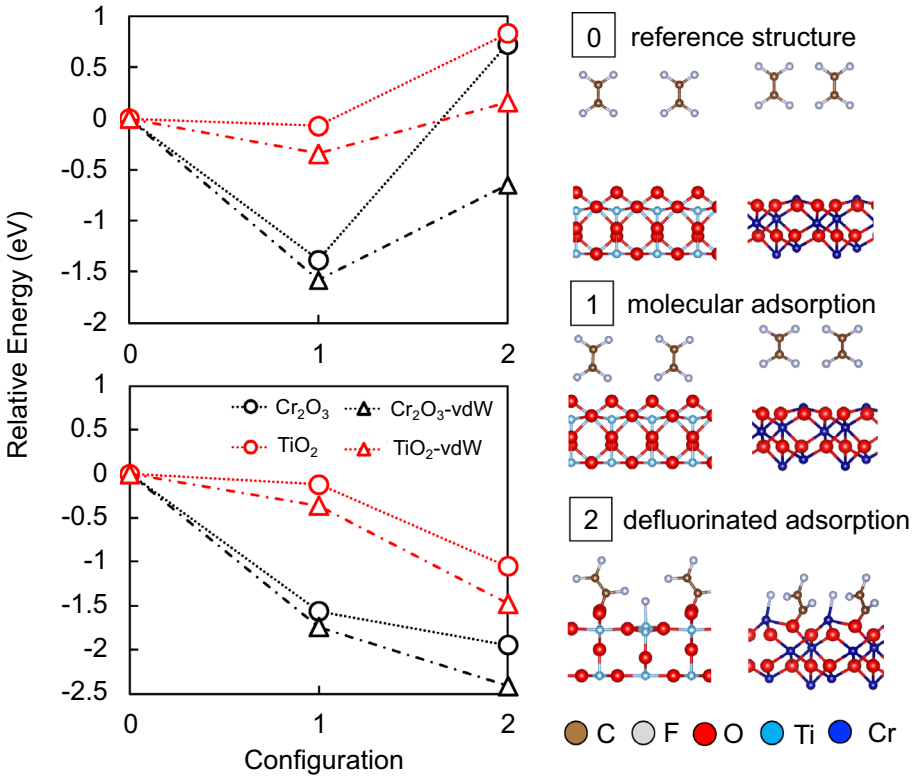

Figure 1. TFE on TiO_2(110) and Cr_2O_3(0001) in 3 different configurations, viz., reference structure (0), molecular adsorption (1), and defluorinated adsorption (2) on the corresponding surfaces. Upper panel corresponds to the relative energies of optimized adsorbates on frozen surfaces. Lower panel corresponds to the relative energies with surface relaxation. (Note stronger TFE adsorption on Cr_2O_3(0001) than on TiO_2(110), having retained energy trend after implementing van der Waals (vdW) correction).

relaxation of the surface. However, the difference in the adsorption energy could be attributed to the difference in the surface oxygen (O)-coordination of the surface metal atoms (Ti and Cr).

In Fig. 2, by inspection, we see that the surface Ti on TiO_2(110) have higher O-coordination than the surface Cr on Cr_2O_3(0001). We attribute the difference in surface reactivity, i.e., adsorption preference, to the difference in surface metal–oxygen ratio. We define this ratio as the number of low coordinated surface metal ions to the fractional number of oxygen atoms bound to it, i.e., 3:7 for TiO_2(110) and 1:1 for Cr_2O_3(0001). To verify this, we have added an additional Cr termination on the surface of Cr_2O_3(0001) (4:3 Cr to O ratio) and found a stronger adsorption of TFE with a pronounced non-planar geometry. As expected, we can enhance TFE adsorption on TiO_2(110) by introducing oxygen vacancies (cf., e.g., Refs.[16–18], and references therein).

It requires energy to break the C–F bond of TFE and, in Fig. 1, we see an endothermic dissociative adsorption of TFE (i.e., Configuration 2, with dissociated C–F bond) on both TiO_2(110) and Cr_2O_3(0001), with respect to the molecular state (Configuration 1). However, upon surface relaxation, the total energy lowers, resulting in a rather exothermic adsorption for C_2F_3 + F on both oxide surfaces (cf., Fig. 1). As mentioned earlier, such surface relaxations are negligible in TFE molecular adsorption. The binding of C_2F_3 on surface O atom and the binding of F on surface metal atom (Ti and Cr) resulted in an upward (coordinate) shift of the interacting surface atoms. By comparison, we can see a greater upward shift of Cr and O towards the vacuum for Cr_2O_3, whereas a relatively smaller relaxation on TiO_2 upon adsorption of the defluorinated TFE (cf., Fig. 3). (Note that the energies from Configuration 0 to 2 on both TiO_2(110) and Cr_2O_3(0001) lowers after considering van der Waals correction (vdW-DFT-D2) in the calculation, as it is expected. Still, the energy trend remains (stronger binding on Cr_2O_3 than on TiO_2).

The relative energy plots suggest that the presence of the metal oxide surfaces lowered the energy needed to break the TFE C–F bond. Note that it requires 5.3 eV to dissociate one F from TFE in vacuum. To explore the possibility of a lowered TFE C–F bond dissociation barrier in the presence of metal-oxides, we implemented a simple dissociation model of TFE using the molecular counterpart of the metal-oxide surfaces. In Fig. 4, we show the calculated potential barriers from the molecular TFE state to the dissociated TFE state on Cr_2O_3 (ca. 1.39 eV) and TiO_2 (ca. 2.16 eV). It can be seen from the simple molecular model that C–F dissociation energy lowers in the presence of metal-oxides. These results indicate the role of the surface as a catalyst to form intermediate defluorinated TFE radicals. In the following, we focus on the adsorption of defluorinated radicals of TFE on Cr_2O_3 and TiO_2 surfaces.

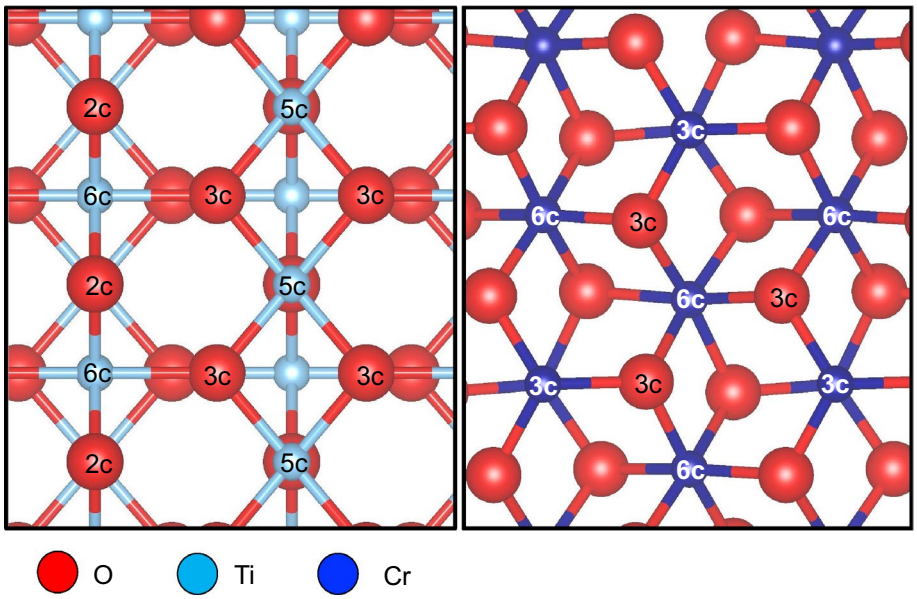

Figure 2. Top view of TiO_2(110) (left panel) and Cr_2O_3(0001) (right panel), with coordination numbers of surface and subsurface atoms indicated. Note the lower coordination number of the surface Cr atoms as compared to the surface Ti atoms.

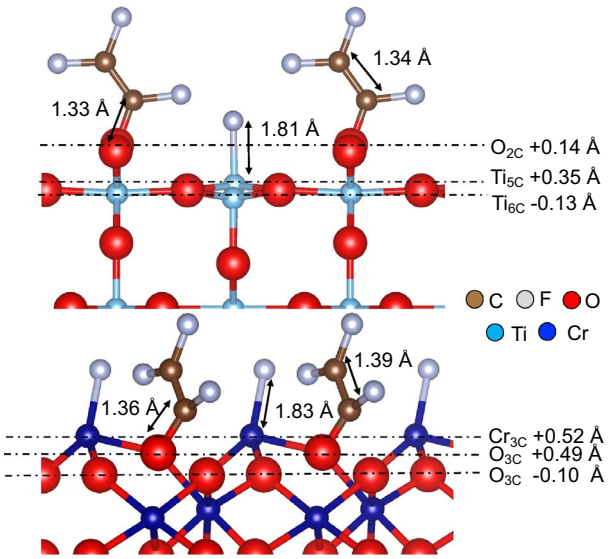

Figure 3. Optimized structure for defluorinated TFE adsorption with the corresponding surface relaxation after adsorption. (+) refers to relaxation of surface atoms towards the vacuum and (−) refers to relaxation of surface atoms towards the bulk. The values are deviations from the clean surface configuration.

Adsorption of defluorinated radicals of TFE on TiO_2(110) and Cr_2O_3(0001). Upon defluorination (cf., e.g., Fig. 1, Configuration 2), the C_2F_3 creates a new bond with surface O atoms and the dissociated F atom adsorbs atop the adjacent transition metal atom. We also see a relatively more stable adsorption on Cr_2O_3(0001) than on TiO_2(110). This results in a higher charge population around the carbon end of C_2F_3 on Cr_2O_3(0001) than on TiO_2(110) (cf., Fig. 5). The relatively higher accumulation of charge from Cr_2O_3 (0.2 e higher) results in a longer C=C bond length (shown in Fig. 3) as compared to that on TiO_2. From the corresponding charge density difference distribution (cf., Fig. 6) electron contribution comes from both surface (oxygen and metal) atoms. We see a more pronounced participation of Cr in TFE radical bonding as compared to Ti shown by the charge gain region (yellow region) between C and Cr surface atom. By plotting the projected density of states (PDOS), after TFE radical bonding, we show a strong hybridization of the C *p* states with the *d* electrons of Cr. This is less evident in the case of TiO_2 where hybridization is mainly through the surface oxygen atom. As mentioned in the previous section, the surface metal–oxygen ratio influences metal-oxide surface reactivity towards TFE adsorp-

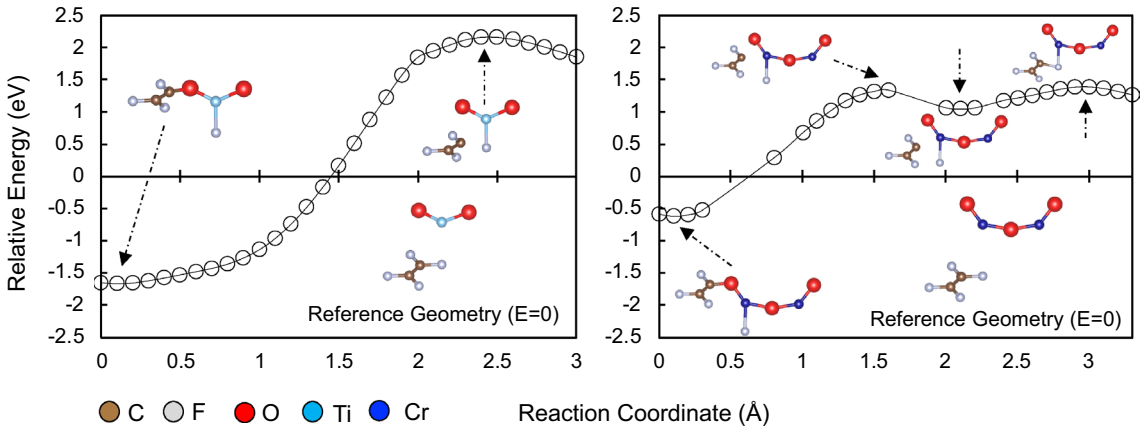

Figure 4. Energies [eV] required to dissociate one F from TFE in the presence of TiO_2 (left panel) and Cr_2O_3 (right panel). Energies given for different configurations (reaction coordinate) relative to the corresponding reference geometries in the insets (E=0). Note that it requires 5.3 eV to dissociate one F from TFE in vacuum.

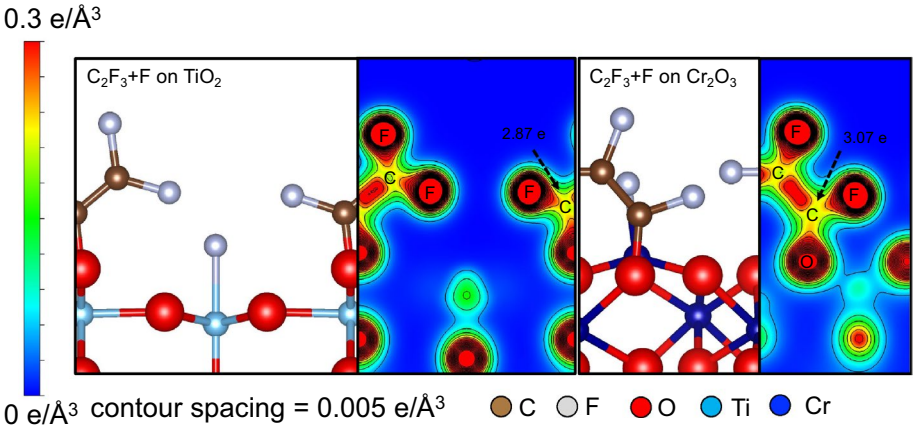

Figure 5. Charge density distributions for TFE adsorbed (dissociated) as C_2F_3 and F on TiO_2(110) (left panel) and on Cr_2O_3(0001) (right panel). A higher accumulation of charge about the C_2F_3 C=C observed on Cr_2O_3(0001).

tion. From the TiO_2(110) geometry, we find the first Ti layer completely enclosed by the octahedral cage of O, resulting in a low surface Ti–O ratio. This accounts for the weak interaction of surface Ti towards C_2F_3. Next, we show in Table 1 the corresponding adsorption energies of CF, CF_2, CF_3, CF_4, C_2F, C_2F_2, C_2F_3 on TiO_2(110) and Cr_2O_3(0001). In general, defluorinated TFE radicals with intact C=C bond show stronger adsorption, and preference for adsorption on Cr_2O_3(0001). We also show that in most cases, radicals with low fluorine content manifest stronger binding on the oxide surfaces. These results indicate that chemical adsorption of the TFE monomer starts with defluorination and adsorption with an intact C=C.

Summary and conclusion

In summary, we have shown that defluorination is necessary to increase chemical bonding between tetrafluoroethylene (TFE) on TiO_2(110) and Cr_2O_3(0001). The metal oxide surface catalyzes defluorination, resulting in the formation of intermediate radicals that bind strongly to the corresponding metal oxide surfaces. As expected, the reactivity of the corresponding metal oxide surfaces depends on the oxygen coordination of metal surface atoms. The surface Cr on Cr_2O_3(0001) has a lower fractional oxygen coordination as compared to the surface Ti on TiO_2(110). As a result, we find stronger bonding of TFE on Cr_2O_3(0001) than on TiO_2(110). This also indicates that introducing oxygen vacancies (cf., e.g., Ref.[16–18], and reference therein), and non-ionizing radiations (cf., e.g., Ref.[19] and references therein) to form intermediate radicals could promote binding of polymers to metals. These results should provide insights for better materials design, specifically towards polymer adhesion on metal-oxide surfaces.

Computational method. To study the adsorption of TFE and its fragments on TiO_2(110) and Cr_2O_3(0001), we performed density functional theory[20,21] (DFT)-based total energy calculations[22–26] using projector augmented wave (PAW) formalism and plane wave basis set (cutoff energy of 550 eV), and Perdew–Burke–Enzer-

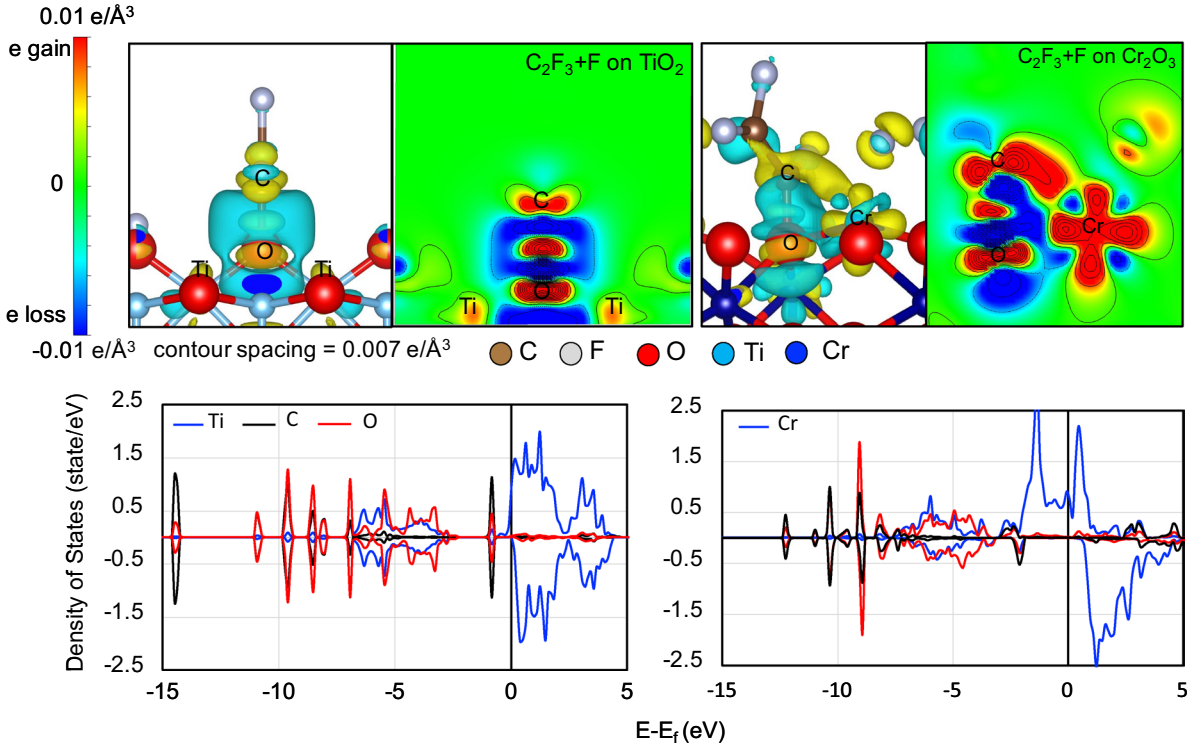

Figure 6. Charge density difference for C_2F_3 + F on TiO_2(110) (upper left panel) and Cr_2O_3(0001) (upper right panel). Yellow to red region indicates electron gain. Light blue to dark blue region indicates electron loss. Projected density of states for C_2F_3 + F on TiO_2(110) (lower left panel) and Cr_2O_3(0001) (lower right panel).

TFE Radical	E_{ad} [eV] on TiO_2(110)	E_{ad} [eV] on Cr_2O_3(0001)
CF	− 2.05	− 4.48
CF_2	− 0.47	− 2.75
CF_3	− 1.66	− 2.2
CF_4	− 0.05	− 0.63
C_2F	− 2.34	− 5.31
C_2F_2	− 2.42	− 5.07
C_2F_3	− 2.02	− 2.53

Table 1. Adsorption energy of defluorinated TFE radicals on Cr_2O_3(0001) and TiO_2(110).

hof (PBE) generalized gradient (GGA) exchange correlation functionals[27,28]. We adopt the Monkhorst and Pack method to perform the Brillouin zone integrations, with (9 × 9 × 1) special *k*-points[29]. To model TiO_2(110) and Cr_2O_3(0001), we used periodically repeated slabs of (2 × 1) and (1 × 1) surface unit cells, respectively, separated by 15 Å thick vacuum region along the surface normal. The lattice constant obtained upon structural optimization for Cr_2O_3(0001) is 5.03 Å and the lattice constants for TiO_2(110) are 2.97 Å and 6.59 Å. These structural geometries are in good agreement with experimental and theoretical studies[30–32]. Each slab consists of 2 layers (7 atomic planes) of O-Ti–O and Cr-O_3-Cr. In the case of Cr_2O_3, we used a Cr terminated surface as it was found to be more stable than other terminations[30]. We performed geometric optimization considering energy convergence of less than 10^{-5} eV and residual forces below 0.01 eV/Å. For the molecular and dissociated adsorption of TFE we implemented both frozen and relaxed surface calculations. We implemented van der Waals correction using DFT-D2 incorporated in the VASP code.

Received: 17 May 2021; Accepted: 20 October 2021
Published online: 03 November 2021

References

1. Li, A., Su, F., Chu, P. K. & Sun, J. Articular cartilage inspired bilayer coating on Ti_6Al_4V alloy with low friction and high load-bearing properties. *Appl. Surf. Sci.* **515**, 146065-1–146110 (2020).
2. Anjum, S. S., Rao, J., Nicholls, J. R. Polymer (PTFE) and shape memory alloy (NiTi) intercalated nano-biocomposites. *IOP Conf. Ser. Mater. Sci. Eng.* **40.** 012006-1-7 (2012).

3. Kim, D. W., Kim, K. T., Lee, D. U., Jung, S. H. & Yu, J. Synergetic enhancement in the reactivity and stability of surface-oxide-free fine Al particles covered with polytetrafluoroethylene nanolayer. *Sci. Rep.* **10**, 14560-1–14610 (2020).
4. Ohkubo, Y., Endo, K. & Yamamura, K. Adhesive-free adhesion between heat-assisted plasma-treated fluoropolymers (PTFE, PFA) and plasma-jet-treated polydimethylsiloxane (PDMS) and its application. *Sci. Rep.* **8**, 18058-1–18111 (2018).
5. Katayama, T. *et al.* Topotactic fluorination of strontium iron oxide thin films using polyvinylidene fluoride. *J. Mater. Chem.* **2**, 5350–5356 (2014).
6. Lange, M. A., *et al.*, A generalized method for high-speed fluorination of metal oxides by spark plasma sintering yields Ta_3O_7F and TaO_2F with high photocatalytic activity for oxygen evolution from water. *Adv. Mater.* 2007434-1-10 (2021).
7. Miwa, K., Takada, N. & Sasaki, K. Fluorination mechanisms of Al_2O_3 and Y_2O_3 surfaces irradiated by high-density CF_4/O_2 and SF_6/O_2 plasmas. *J. Vac. Sci. Technol. A* **27**, 831–835 (2009).
8. Jiang, H. *et al.* Passivated metal oxide n-type contacts for efficient and stable organic solar cells. *ACS Appl. Energy Mater.* **3**, 1111–1118 (2020).
9. Liu, S., Ho, S., Chen, Y. & So, F. Passivation of metal oxide surfaces for high-performance organic and hybrid optoelectronic devices. *Chem. Mater.* **27**, 2532–2539 (2015).
10. Hirai, D., Sawai, O., Nunoura, T. & Hiroi, Z. Facile synthetic route to transition metal oxyfluorides via reactions between metal oxides and PTFE. *J. Fluorine Chem.* **209**, 43–48 (2018).
11. Kitamura, K., Nishiyama, Y., Fujimoto, S. & Otsuka, N. Stress and adhesion of protective oxide scales on stainless steels and RE effects. *ISIJ Int.* **59**, 1642–1649 (2019).
12. Wen, M., Wen, C., Hodgson, P. & Li, Y. Improvement of the biomedical properties of titanium using SMAT and thermal oxidation. *Colloid Surface B* **116**, 658–665 (2014).
13. Mei, L., Yan, D., Xie, S., Lei, Z. & Ge, X. Effects of Cr_2O_3 active agent on the weld process dynamic behavior and joint comprehensive properties of fiber laser welded stainless steel thick plate. *Opt. Laser Eng.* **128**, 106027-1–106114 (2020).
14. Hori, K., Fujimoto, S., Togashi, Y., Kuroki, T. & Okubo, M. Improvement in molecular-level adhesive strength of PTFE film treated by atmospheric plasma combined processing. *IEEE T. Ind. Appl.* **55**, 825–832 (2019).
15. Vogt, K. W., Kohl, P. A., Carter, W. B., Bell, R. A. & Bottomley, L. A. Characterization of thin titanium oxide adhesion layers on gold resistivity, morphology, and composition. *Surf. Sci.* SSC05379-1-11 (1993).
16. Shukri, G. & Kasai, H. Density functional theory study of ethylene adsorption on clean anatase TiO_2(001) surface. *Surf. Sci.* **619**, 59–66 (2014).
17. Linh, N. H., Nguyen, T. Q., Diño, W. A. & Kasai, H. Effect of oxygen vacancy on the adsorption of O_2 on anatase TiO_2(001): A DFT-based study. *Surf. Sci.* **633**, 38–45 (2015).
18. Shukri, G., Diño, W. A., Dipojono, H. K., Agusta, M. K. & Kasai, H. Enhanced molecular adsorption of ethylene on reduced anatase TiO_2(001): Role of surface O-vacancies. *RSC Adv.* **6**, 92241–92251 (2016).
19. Katayama, S. & Kawahito, Y. Laser direct joining of metal and plastic. *Script. Mater.* **59**, 1247–1250 (2008).
20. Kohn, W. & Sham, L. J. Self-consistent equations including exchange and correlation effects. *Phys. Rev.* **140**, A1133–A1138 (1965).
21. Hohenberg, P. & Kohn, W. Inhomogeneous electron gas. *Phys. Rev.* **136**, B864–B871 (1964).
22. Kresse, G. & Furthmüller, J. Efficiency of ab-initio total energy calculations for metals and semiconductors using a plane-wave basis set. *Comput. Mater. Sci.* **6**, 15–50 (1996).
23. Kresse, G. & Furthmüller, J. Efficient iterative schemes for ab initio total-energy calculations using a plane-wave basis set. *Phys. Rev. B* **54**, 11169–11186 (1996).
24. Kresse, G. & Hafner, J. Ab initio molecular dynamics for liquid metals. *Phys. Rev. B* **47**, 558–561 (1993).
25. Kresse, G. & Hafner, J. Ab initio molecular-dynamics simulation of the liquid-metal-amorphous-semiconductor transition in germanium. *Phys. Rev. B* **49**, 14251–14269 (1994).
26. Kresse, G. & Joubert, D. From ultrasoft pseudopotentials to the projector augmented-wave method. *Phys. Rev. B* **59**, 1758–1775 (1999).
27. Perdew, J. P., Chevary, J. A., Vosko, S. H., *et al.* Atoms, molecules, solids, and surfaces: Applications of the generalized gradient approximation for exchange and correlation. *Phys. Rev. B* **46** 6671–6687 (1992); *Phys. Rev. B* **48** 4978 (1993) (Erratum).
28. Perdew, J. P., Burke, K. & Ernzerhof, M. Generalized gradient approximation made simple. *Phys. Rev. Lett.* **77**, 3865–3868 (1996); *Phys. Rev. Lett.* **78**, 1396 (1997) (Erratum).
29. Monkhorst, H. J. & Pack, J. D. Special points for Brillouin-zone integrations. *Phys. Rev. B* **13**, 5188–5192 (1976).
30. Rehbein, C., Harrison, N. M. & Wander, A. Structure of the a-Cr_2O_3 surface: An ab initio total-energy study. *Phys. Rev. B* **54**, 14066–14070 (1996).
31. Onishi, H., Fukui, K. & Iwasawa, Y. Atomic-scale surface structures of TiO_2(110) determined by scanning tunneling microscopy: A new surface-limited phase of titanium oxide. *Bull. Chem. Soc. Jpn.* **68**, 2447–2458 (1995).
32. Shirasawa, T., Voegeli, W., Arakawa, E., Takahashi, T. & Matsushita, T. Structural change of the rutile–TiO_2(110) surface during the photoinduced wettability conversion. *J. Phys. Chem. C* **120**, 29107–29115 (2016).
33. Momma, K. & Izumi, F. VESTA 3 for three-dimensional visualization of crystal, volumetric and morphology data. *J. Appl. Crystallogr.* **44**, 1272–1276 (2011).

Acknowledgements

This work is supported in part by MEXT Grants-in-Aid for Scientific Research (JP20H02638, JP20K21171, JP17H01057) and METI Strategic Basic Technology Support Project (2018). Some of the numerical calculations presented here were done using the computer facilities at the following institutes: CMC (Osaka University), ISSP, KEK, NIFS, and YITP. Structures are drawn using the VESTA package (ver.3.5.7)[33].

Author contributions

K.W., H.N., T.K., and W.A.D. conceived the calculations. J.S.G. and N.E.A.S. performed the DFT calculations. J.S.G. and W.A.D. drafted the manuscript. All Authors contributed to the analyses of results and review of the manuscript.

Competing interests

The authors declare no competing interests.

Additional information

Correspondence and requests for materials should be addressed to J.S.G., W.A.D. or K.W.

Reprints and permissions information is available at www.nature.com/reprints.